

Including the invisible: Deep depth-integrated chlorophyll estimates from remote sensing may assist in identifying biologically important areas in oligotrophic coastal margins

Renée P. Schoeman¹, Christine Erbe¹, and Robert D. McCauley¹

5 ¹Centre for Marine Science and Technology, Curtin University, Bentley, Western Australia 6102, Australia

Correspondence to: Renée P. Schoeman (renee.koper@postgrad.curtin.edu.au)

Abstract. Surface chlorophyll from satellite remote sensing is a common predictor variable in marine animal habitat studies but fails to capture deep chlorophyll maxima (DCM) that are unambiguous in persistently stratified water columns. DCMs are also present within the meso-oligotrophic marine environment of Western Australia and have been hypothesised to be an important feature for the growth and maintenance of regional krill populations on which locally endangered pygmy blue whales feed. This study used ~8500 vertical ocean glider profiles collected between 2008 and 2021 to better understand the broad-scale temporal presence of DCMs and their characteristics in West Australian waters. Our results show that DCMs are predominantly present from September to April, with a high proportion of biomass maxima within the euphotic zone in September and March. In summer, DCMs deepen and settle below the euphotic zone. The latter results in a balanced presence of biomass and photo-acclimation maxima, placing Western Australian waters in a unique biogeographical biome. In addition, since DCMs in summer contribute to over 50 % of water column-integrated chlorophyll below the euphotic zone, our results are in support of hypotheses regarding the importance of the DCM for local krill and highlight the need to develop methods to include water column-integrated chlorophyll estimates in habitat models. Linear regression analyses show that this could be achieved through the extension of previously known relationships between surface and water column-integrated chlorophyll over the euphotic zone to twice the euphotic zone depth (i.e., deep depth-integrated chlorophyll). While using water column-integrated chlorophyll estimates from satellite remote sensing has its challenges, it is currently the only means to include DCMs in habitat models fitted to large temporal- or spatial-scale animal presence data.

1 Introduction

Phytoplankton are instrumental in providing energy to higher trophic levels of aquatic ecosystems. Their biomass is mostly quantified in terms of chlorophyll-a (hereafter called chlorophyll), from which primary productivity is derived, and areas with potentially high prey availability for higher trophic levels are identified (Huot et al., 2007; Hobday and Hartog, 2014). Indeed, several studies identified chlorophyll as a significant predictor variable of foraging habitat and hot spots for primary consumers (e.g., Schmidt et al., 2012; Hellesey et al., 2020) and higher trophic levels (e.g., Suryan et al., 2012; Palacios et al., 2019; Salgado Kent et al., 2020; Speakman et al., 2020).

30 While chlorophyll levels can be quantified using several techniques (i.e., visual assessment of ocean colour, spectrophotometry, fluorometry, and chromatography; Parsons and Strickland, 1963; Yentsch and Menzel, 1963; Jeffrey, 1974; Gieskes and Kraay, 1977; Jeffrey et al., 1999), phytoplankton biomass and productivity studies flourished with the launch of the first satellite remote sensing ocean colour mission in 1978 (Hovis et al., 1980; McClain, 2009). Not only has satellite remote sensing generated a near-continuous chlorophyll dataset with high spatial resolution (Groom et al., 2019), the data are also widely accessible, resulting in the inclusion of satellite-derived chlorophyll—almost as a default—in studies aiming to identify crucial marine animal foraging areas. Yet, satellite remote sensing is restricted to the upper water column (2–39 m; Organelli et al., 2017) and likely excludes Deep Chlorophyll Maxima (DCMs; Gordon and McCluney, 1975; Smith, 1981), which may—at least in some areas—be an essential feature to support higher-order foraging efforts (Rennie et al., 2009a; Scott et al., 2010).

40 DCMs are observed throughout the global oceans, with a year-round and consistent presence in tropical and most sub-tropical regions (Mignot et al., 2014; Bock et al., 2022; Quartly et al., 2023). Seasonal patterns of occurrence become more evident from temperate to high-latitude regions (Cornec et al., 2021), during which DCMs are present in summer but tend to break down or occur less frequently in winter (e.g., Mignot et al., 2014; Baldry et al., 2020; Bock et al., 2022). In well-studied tropical and temperate regions, DCM formation has been linked to permanent or seasonally stable stratified water conditions (Cornec et al., 2021), with light and nutrient availability driving the formation of true phytoplankton biomass maxima (i.e., deep biomass maxima, DBM) and deep photo-acclimation maxima (DAM; Mignot et al., 2014; Cullen, 2015). While DAMs result from an increased chlorophyll-to-carbon ratio because of low-light adaption rather than an increase in transferrable carbon (Steele, 1962, 1964), both DBMs and DAMs may contribute to water column productivity adequately enough to be of relevance to higher trophic levels (e.g., Weston et al., 2005; Fernand et al., 2013; Mignot et al., 2014; Marañón et al., 2021).

50 The marine habitat of Western Australia is characterised by a cross-shelf gradient in surface chlorophyll values decreasing from winter maxima $\sim 1 \text{ mg m}^{-3}$ along the coast to $\sim 0.4 \text{ mg m}^{-3}$ in offshore waters (i.e., $>300 \text{ m}$ deep; Lourey et al., 2006; Fearn et al., 2007; Hanson et al., 2007a; Koslow et al., 2008). However, surface chlorophyll values vary seasonally and, offshore, generally do not exceed 0.1 mg m^{-3} in summer (Hanson et al., 2005a, 2005b; Lourey et al., 2006; Koslow et al., 2008). These intermittent oligotrophic conditions result from the poleward flowing Leeuwin Current, which transports warm, low salinity, and low nutrient water along the continental shelf break (Cresswell and Golding, 1980). Despite seasonal variation in current strength with minimum geostrophic flow in January–February (Feng et al., 2003), the Leeuwin Current generally suppresses nutrient upwelling by strong south-westerly winds that blow in spring and summer (i.e., September–February; Rennie et al., 2006, 2009b). Stratification weakens or may break down in late autumn and winter, which has been linked to an initial deepening of the mixed layer by an intensification of the Leeuwin Current strength (i.e., peak strength in June–July; Feng et al., 2003) and subsequent maintenance of turbulent conditions by north-westerly winter storms and enhanced eddy kinetic energy (Koslow et al., 2008; Rennie et al., 2006).

DCMs form in the vertically stratified water column of Western Australia in summer at a depth between 50 m and 120 m offshore, shoaling to the surface or seabed on the continental shelf (Hanson et al., 2005b, 2007a; Twomey et al., 2007; Koslow

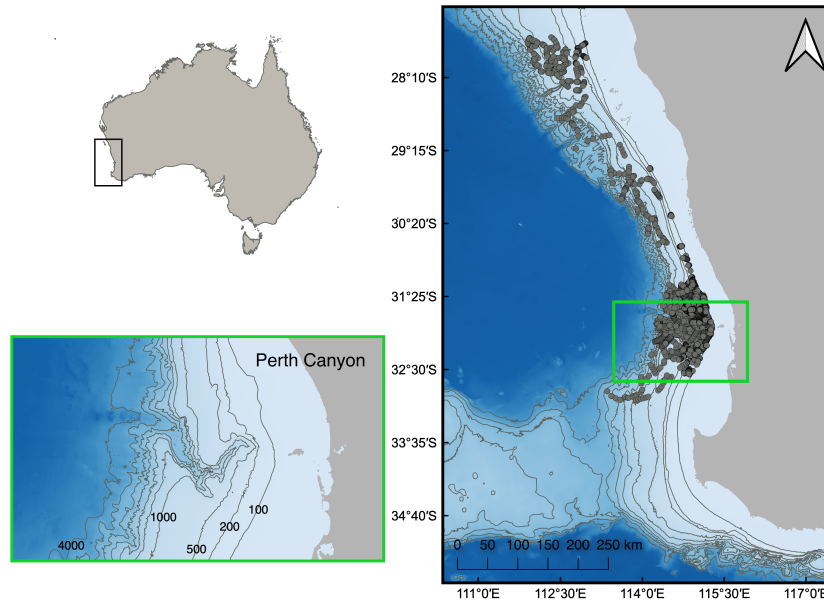
et al., 2008; Rennie et al., 2009a; Chen et al., 2019). While DCMs tend to break down around the shelf edge in late autumn and winter (Chen et al., 2019), they may persist offshore at shallower depths (15–70 m; Hanson et al., 2005b; Koslow et al., 2008). Previous studies have confirmed that the DCM is often a biomass maximum (Hanson et al., 2005b, 2007a; Rennie et al., 2009a), responsible for 30–70 % of total water column productivity (Hanson et al., 2007a). More importantly, the DCM may be a vital feature for *Euphausia recurva*, the most abundant krill species along the southwest Australian coast, including the Perth Canyon (Sutton and Beckley, 2016). *E. recurva*, in turn, is the common prey for locally endangered pygmy blue whales (*Balaenoptera musculus breviceauda*) known to feed around the Perth Canyon’s head, northern rim, and plateau in waters 300–600 m deep (McCauley et al., 2004; Rennie et al., 2009a) and along the continental shelf break (200 m contour line; Owen et al., 2016) from February–June (peak presence February–March; McCauley et al., 2004; Erbe et al., 2015). Acoustic backscatter data from the Perth Canyon in late summer (February) suggests that krill gather at 300–500 m depth during the day, rising to the DCM at night to feast on phytoplankton prey (Rennie et al., 2009a; McCauley and Cato, 2016). Rennie et al. (2009a) highlighted that pygmy blue whales can only be expected to forage in areas where the metabolic gain from foraging supersedes the energy expenditure related to lunge feeding. Based on CTD analyses and numerical and phytoplankton studies, the authors hypothesised that the krill population of Western Australia is maintained throughout the year by increased productivity in both winter (related to surface blooms) and summer (related to subsurface blooms near the DCM). Sutton (2015) supported this observation with fatty acid and stable isotope analysis on krill caught in the Perth Canyon in April (i.e., prior to the annual increase in surface phytoplankton in May), which did not reflect a diet of surface phytoplankton. Its apparent significance highlights the need to gain a better understanding of the broad-scale seasonal patterns in DCM formation and potential underlying processes and to consider the inclusion of DCMs in phytoplankton biomass estimates and marine animal habitat models.

While it is known that DCMs form in Western Australian waters, our knowledge of their seasonal presence and characteristics (e.g., DCM depth, type and width, maximum chlorophyll concentration at depth, etc.) is limited to cross-continental shelf time series (e.g., Fearn et al., 2007; Koslow et al., 2008; Chen et al., 2019) and broad-scale temporally restricted analyses (e.g., Hanson et al., 2005b, 2007; Twomey et al., 2007; Thompson et al., 2011). This study used 14 years of ocean glider data to assess broad-scale temporal patterns in water column characteristics, DCM formation, and DCM characteristics in the meso-oligotrophic marine environment of Western Australia, focusing on the area between 27.5° S and 33.8° S where the Perth Canyon lies. In addition, while several studies have shown that surface chlorophyll values measurable by satellite remote sensing can estimate water column-integrated chlorophyll over the euphotic zone (depth over which Photosynthetically Active Radiation, PAR, decreases to 1 % of its surface value $Z_{1\%PAR}$, hereafter referred to as “depth-integrated chlorophyll”; Morel and Berthon, 1989; Uitz et al., 2006; Frolov et al., 2012), these studies were based on samples from open oceanic regions or a regional eutrophic continental margin. We, therefore, assessed whether relationships between surface and water column-integrated chlorophyll values were similarly present in waters of Western Australia for potential use in habitat models.

2 Methods

2.1 In situ ocean glider data retrieval

We downloaded in situ ocean glider data from the Australian Ocean Data Network (AODN) portal. Data were collected between 21 June 2008 and 12 July 2022 by the Integrated Marine Observing System's Australian National Facility for Ocean
100 Gliders (IMOS-ANFOG; IMOS, 2023) within an area extending from 27.5° S to 33.8° S and 109.7° E to 115.4° E (Fig. 1). Within this area, the Perth Canyon is located at ~32° S. Ocean glider missions were conducted each year but with varying intensity between years and concentrated around the continental shelf, shelf break, and deeper waters surrounding the Perth Canyon (see Supplementary Fig. S1 and S2 for illustrations of temporal and spatial coverage). Consequently, after the filtering process described below and in Sections 2.2 and 2.3, data were spatially clustered between 31.6° S to 32.1° S and 114.9° E to
105 115.3° E, collected between 25 July 2008 and 13 December 2021, and obtained from waters with a mean water depth of 422 m (Fig. 1). All ocean gliders were equipped with a Sea-Bird Conductivity-Temperature-Depth sensor (CTD: models CTD41CP, GPCTD, or SBE_CT) and a WET Labs ECO Puck optical sensor pack (models BBFL2S, BBFL2VMT, FLBBCDSLK, or FLBBCDSLK), including a fluorometer and backscattering sensor (650-700 nm, 117° centroid angle). All downloaded data were pre-processed and quality-controlled by IMOS, which included the conversion of raw sensor counts into chlorophyll and
110 particle backscatter coefficient (bbp) parameters with instrument-specific calibration coefficients and dark count values (Mantovanelli and Thomson, 2016; Woo and Gourcuff, 2023). Chlorophyll dark count values were corrected for any mission with >1% of negative values (Woo and Gourcuff, 2023). Quality control processes included automatic sensor drift corrections; automatic flagging of impossible location, date, and range values; manual flagging of measurements affected by biofouling or sensor malfunction; and manual flagging of near-surface measurements (<0.5 m). Further data processing was done in
115 MATLAB (Version 2022b; The MathWorks Inc., 2022), while statistical analyses were performed in R and RStudio Statistical Software (V4.2.0 and V2023.03.0, respectively; R Core Team, 2022).



120 **Figure 1: Ocean glider night-time vertical profile samples (grey circles) collected between the 100 m and 3000 m bathymetry contour lines off southwestern Australia, with the Perth Canyon situated at 32° S (within green square). Bathymetry contour lines delineate isobaths at 100 m, 200 m, and 500–4000 m in 500 m increments.**

2.2 Ocean glider depth profile extraction

Information extracted from ocean glider data samples included UTC date and time, latitude (DD), longitude (DD), sampling depth (m), chlorophyll concentration (mg m^{-3}), temperature ($^{\circ}\text{C}$), practical salinity (‰), pressure (dbar), profile phase (i.e., descent, inflexion, or ascent), and where available, particle backscattering coefficient data (m^{-1}). We filtered ocean glider data based on IMOS quality control flags to retain data points of which each variable was flagged as good data, probably good data, value adjusted by the quality control centre, or interpolated value (i.e., flags 1, 2, 5, and 8, respectively; Woo and Gourcuff, 2023). Data were interpolated between each decent and subsequent ascent phase to extract one vertical profile to the deepest recorded depth. Only profiles with at least one observation within the first 10 m of the water column were retained (Uitz et al., 2006). We then calculated the sun's angle relative to the horizon for each profile with the *suncalc* R-package (Thieurmel and Elmarhraoui, 2022) and removed all profiles obtained with the sun above the horizon (i.e., day-time profiles) from further analyses to avoid underestimating surface chlorophyll concentrations because of non-photochemical quenching (Roesler and Barnard, 2013). Finally, bathymetry data extracted from the Australian bathymetry and topography grid (Whiteway, 2009) were used to omit all samples from waters <100 m and >3000 m deep. This was done to ensure that data analyses were focussed on a section of the continental margin over which pygmy blue whales have been observed (McCauley et al., 2004; Double et al., 2014; Thums et al., 2022). After this initial filtering process, 21303 profiles were kept for further processing.

130

135

2.3 Temporal patterns in water column conditions

The prevalence of DCMs and relationship between surface and depth-integrated chlorophyll concentrations differ between mixed and stratified water columns (Morel and Berthon, 1989; Uitz et al., 2006; Cullen, 2015). We, therefore, split profiles between mixed and stratified water conditions based on the euphotic zone depth (i.e., $Z_{eu} = Z_{1\%PAR}$; see Table 1 for a list of symbols) and mixed layer depth (MLD) as positive values below the surface. Following Uitz et al. (2006), we classified waters as mixed when $Z_{eu} < MLD$ and stratified when $Z_{eu} > MLD$. The euphotic zone depth for each profile was derived from the vertical chlorophyll distribution by progressive trapezoidal integration of chlorophyll over depth (Z ; Morel and Berthon, 1989). For each sampling depth (Z_i), we converted depth-integrated chlorophyll concentrations to euphotic zone depth with formulae in Morel and Maritorena (2001) until $Z_{eu} < Z_i$ (Morel and Berthon, 1989). The exact euphotic zone depth was then calculated by interpolating Z_{eu} between Z_i and Z_{i-1} to find where Z equalled Z_{eu} (Morel and Berthon, 1989). Profiles that did not reach the euphotic zone depth were discarded, leaving 8486 profiles for statistical analyses.

Table 1: List of symbols used in this study and their denotation.

Symbol	Denotation	Unit
Bbp_{max}	Maximum particle backscattering coefficient within 20 m of the deep chlorophyll maximum.	m^{-1}
Bbp_{min}	Minimum particle backscattering coefficient within the top 15 m of the water column.	m^{-1}
Chl_{HPLC}	Average chlorophyll concentration within the top 10 m of the water column obtained from High-Performance Liquid Chromatography analyses of in situ water samples.	$mg\ m^{-3}$
Chl_{max}	Maximum chlorophyll concentration within the top 300 m of the water column.	$mg\ m^{-3}$
Chl_{MODIS}	Surface chlorophyll concentration retrieved with the OCI algorithm from ocean colour measurements by MODIS-aqua.	$mg\ m^{-3}$
Chl_{zeu}	Total chlorophyll concentration integrated over the euphotic layer.	$mg\ m^{-2}$
Chl_{zeu2}	Total chlorophyll concentration integrated over twice the euphotic layer depth.	$mg\ m^{-2}$
Chl_{zpd}	Average chlorophyll concentration within the first optical depth.	$mg\ m^{-3}$
DCM_{width}	Width of the deep chlorophyll maximum; calculated as the difference in depth between the shallow- and deep half-peak depths.	m

Z	Depth below the water surface (positive).	m
$Z_{1\%}^{\text{PAR}}$	Depth at which the Photosynthetically Active Radiation (PAR) is 1 % of its surface value.	m
Z_{DCM}	Depth of Chl_{max} .	m
$Z_{\text{DCM}50\text{d}}$	Closest depth to Z_{DCM} at which chlorophyll concentration decreased to 50 % of Chl_{max} ; deep half-peak width.	m
$Z_{\text{DCM}50\text{u}}$	Closest depth to Z_{DCM} at which chlorophyll concentration increased to 50 % of Chl_{max} ; shallow half-peak width.	m
Z_{eu}	Bottom depth of the euphotic layer (in this study equal to $Z_{1\%}^{\text{PAR}}$).	m
MLD	Bottom depth of the water column mixed layer.	m

Raw temperature, salinity, and pressure data were converted to potential temperature and density values with the Gibbs-SeaWater (GSW) Oceanographic Toolbox (IOC et al., 2010; McDougall and Barker, 2020) to calculate the mixed layer depth. Here, we define the mixed layer depth as the first depth at which either the potential temperature differed by 0.2 °C from the reference potential temperature or the potential density exceeded the reference potential density by 0.03 kg m⁻³, with samples taken at 10 m depth as reference values (de Boyer Montégut et al., 2004; Boettger et al., 2018).

2.4 Temporal patterns in DCM presence, classification, and characteristics

Cornec et al. (2021) identified values and depths of maximum chlorophyll and particle backscatter coefficient data from smoothed vertical profiles before locating the nearest equivalent maximum chlorophyll (Chl_{max}) and particle backscatter coefficient (Bbp_{max}) on the unsmoothed profiles. Maxima values from the unsmoothed profiles were then compared to values within the top 15 m to identify whether a DCM was present (i.e., Chl_{max} exceeded twice the median chlorophyll concentration over the top 15 m) and whether a DCM was a DBM (i.e., Bbp_{max} exceeded 1.3 times the minimum particle backscattering coefficient in the top 15 m) or a DAM. Our methods followed those of Cornec et al. (2021) with a minor modification to the smoothening process. Chlorophyll profiles were smoothened with a 5, 7, or 11-point moving median corresponding to median profile depth resolutions of ≥ 3 m, < 3 m but > 1 m, and ≤ 1 m, respectively (Schmechtig et al., 2023). Particle backscatter coefficient profiles were smoothed with an 11-point moving median, followed by an 11-point moving mean. The depth of Chl_{max} (Z_{dcm} ; DCM peak depth), shallow half-peak depth ($Z_{\text{dcm}50\text{u}}$), and deep half-peak depth ($Z_{\text{dcm}50\text{d}}$) were also extracted. The DCM width ($\text{DCM}_{\text{width}}$) was calculated as the depth range between the shallow and deep half-peak depths (i.e., $Z_{\text{dcm}50\text{d}} - Z_{\text{dcm}50\text{u}}$). Trends in the position of the DCM peak and width relative to the euphotic zone were assessed by calculating their

relative positions as $\text{Chl}_{\text{max}}/Z_{\text{eu}}$ and $Z_{\text{dem50d}}/Z_{\text{eu}}$, respectively, where values <1 were indicative of a peak chlorophyll value or full half-peak width within the euphotic zone.

2.5 Relationships between surface and water column-integrated chlorophyll

170 Relationships between surface and water column-integrated chlorophyll concentrations were assessed based on methods described in earlier publications (Morel and Berthon, 1989; Uitz et al., 2006; Frolov et al., 2012). We calculated surface chlorophyll values—assumed measurable by satellite—as the average chlorophyll concentration over the first optical depth (i.e., Chl_{zpd} ; Uitz et al., 2006), where the first optical depth refers to $Z_{\text{eu}}/4.6$ (Gordon and McCluney, 1975). Since $Z_{1\%}^{\text{PAR}}$ may underestimate the biological compensation depth at which the rate of photosynthesis equals that of autotrophic respiration and
175 thus, the depth of the productive layer, we integrated chlorophyll concentrations via trapezoidal integration over the euphotic zone (i.e., depth-integrated chlorophyll; Chl_{zeu}) and where possible, twice the euphotic zone depth (hereafter referred to as “deep depth-integrated chlorophyll”; $\text{Chl}_{\text{zeu}2}$). The latter differs from Uitz et al. (2006), who integrated chlorophyll over a maximum of one-and-a-half times the euphotic zone depth because preliminary analysis indicated that 34.8 % of DCM half-peak widths extended beyond that limit (see Supplementary Fig. S3 for a DCM full-width inclusion curve).

180 Relationships were quantified using linear regression analyses on \log_{10} transformed data, conducted separately for mixed and stratified water conditions. Previous publications used two regression lines to quantify the relationship in stratified waters because of a change in slope at surface chlorophyll values $\sim 1 \text{ mg m}^{-3}$ (Morel and Berthon, 1989; Uitz et al., 2006; Frolov et al., 2012). While preliminary data analysis revealed a similar change in slope in this study, the change appeared seasonal and related to a change in the shape of vertical chlorophyll profiles from ones with low surface chlorophyll values and a pronounced
185 DCM to ones with higher surface chlorophyll values without a DCM (Fig. 2). Thus, we carried out one regression analysis for stratified water conditions from September until April and one for stratified water conditions from May until August. For brevity, the two seasons will be referred to as summer-transition and mid-winter, respectively. We evaluated all models with the Mean Absolute Error (MAE) and bias metrics because of tailed distributions in model residual plots (Chai and Draxler, 2014; Seegers et al., 2018; Hodson, 2022). Both metrics were transformed from linear to multiplicative values for ease of
190 interpretation (Seegers et al., 2018). The slope and intercept of the linear regression were converted into a power-law regression to describe the non-linear relationship between non-transformed surface and water column-integrated chlorophyll values.

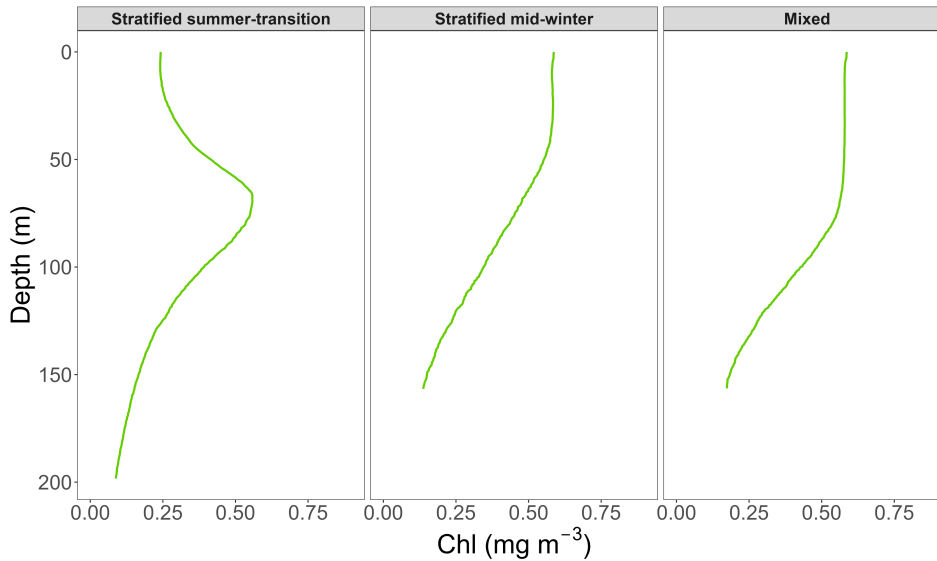
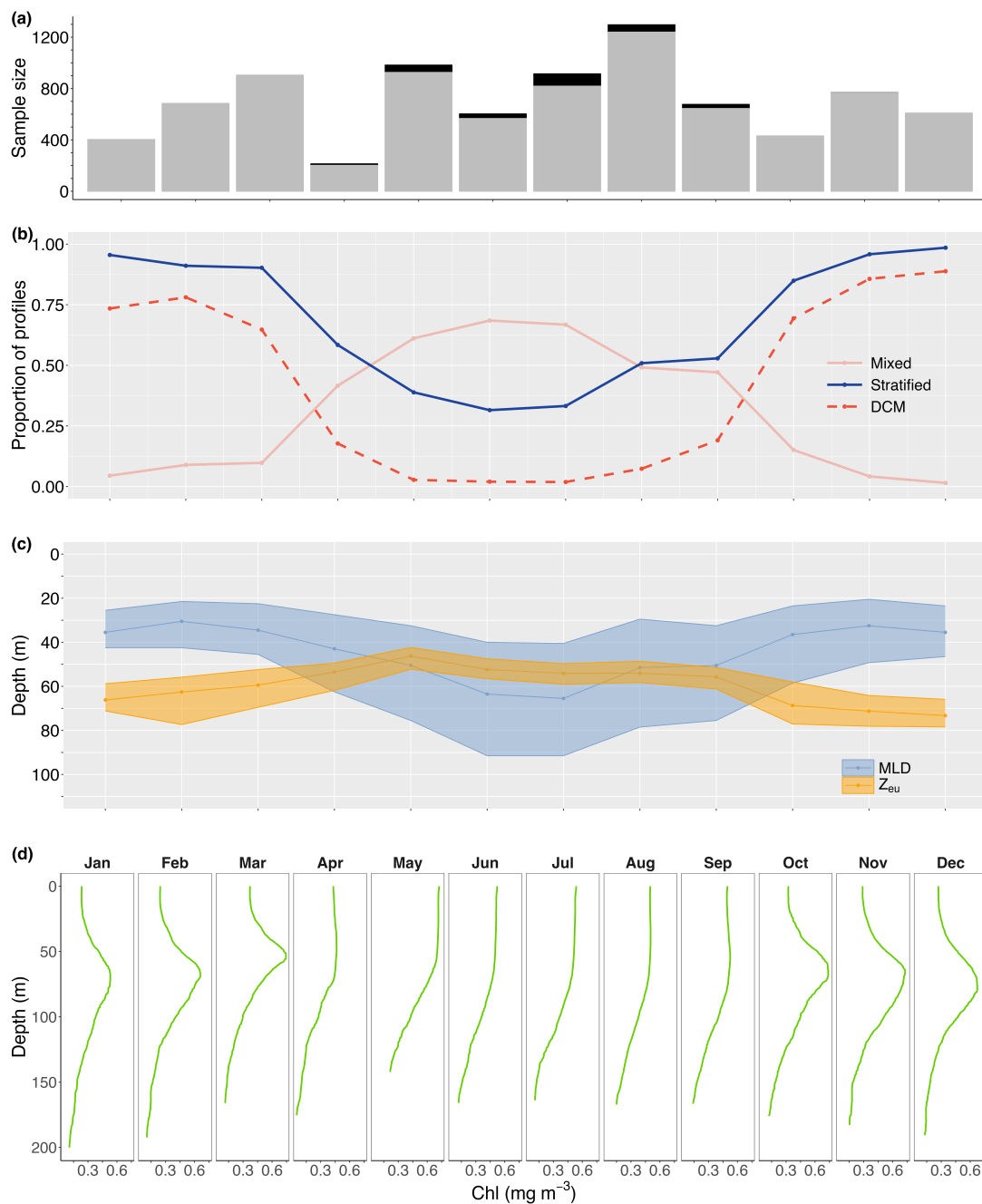


Figure 2: Median vertical chlorophyll profiles for (a) stratified summer-transition (September–April), (b) stratified mid-winter (May–August), and (c) mixed water conditions.

195 3 Results

3.1 Temporal patterns in water column conditions

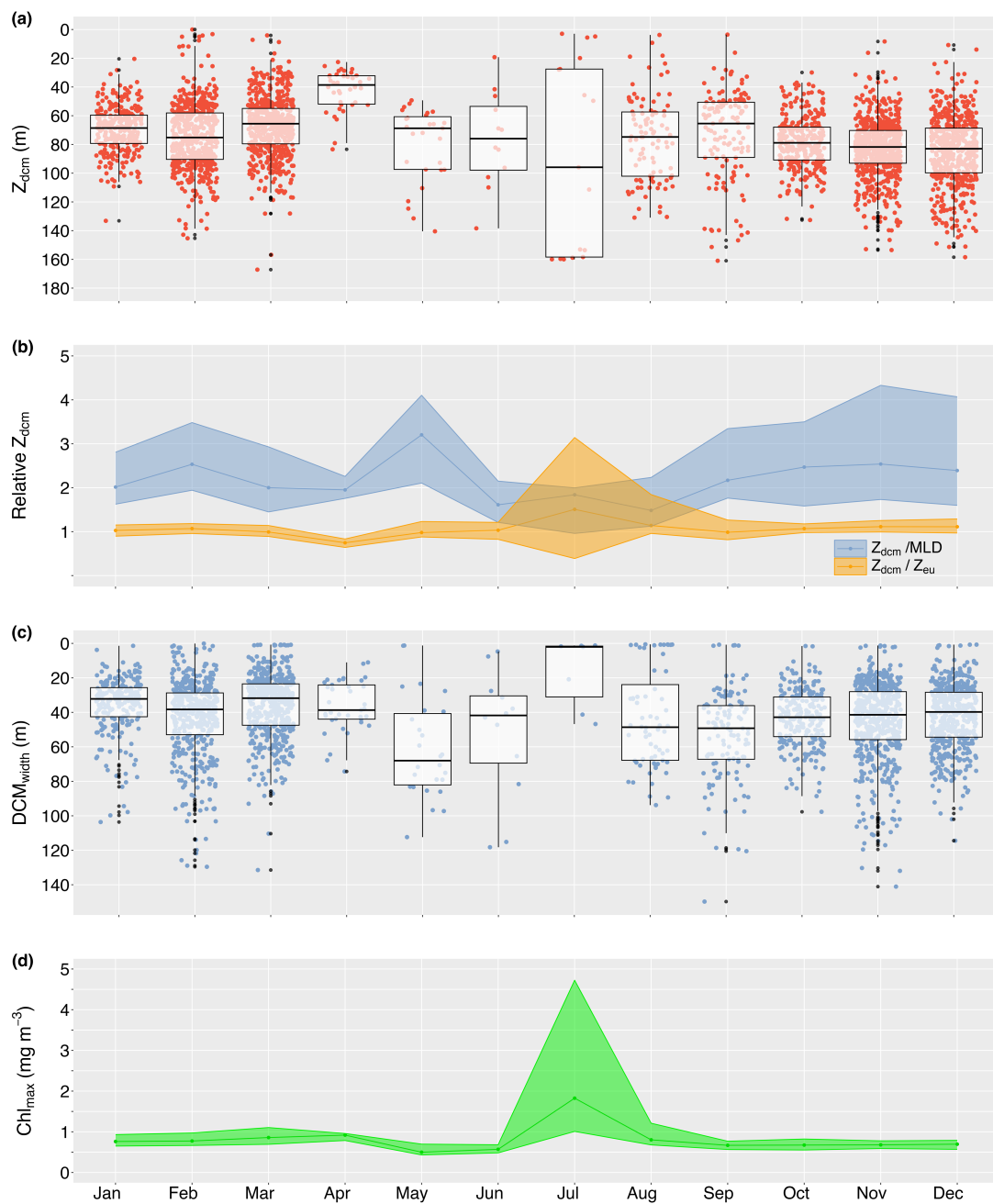
We extracted 5543 and 2943 profiles from stratified and mixed water conditions, respectively. Stratified water conditions dominated over the warm late spring, summer, and early autumn months (October–March; $\geq 85\%$ of profiles), declining to $< 39\%$ over May–July when mixed water conditions prevailed (Fig. 3b). Transition conditions were present in April, August, and September, with an approximate 50:50 occurrence of stratified and mixed water conditions. The change in prevailing water condition was predominantly caused by a deepening of the median mixed layer depth from 30.5 m (IQR 21.0 m) in February to 65.5 m (IQR 51.0 m) in July (Fig. 3c). In contrast, the euphotic zone depth moved closer to the surface from a median of 73.3 m (IQR 12.5 m) in December to 46.3 m (IQR 10.9 m) in May (Fig. 3c).



205 **Figure 3:** Number of profiles extracted for each month (black bars) overlain with the number of profiles for which the mixed layer depth (MLD) was reached (grey bars; panel a). For each month, the proportion of vertical profiles extracted from mixed (solid pink line) and stratified (solid blue line) water conditions is provided in panel (b), along with the proportion of profiles characterised by a DCM (red dashed line; panel b) and the seasonal change in median (with 25th and 75th quartiles as shaded areas) euphotic zone (Z_{eu}) and mixed layer depth (c). Panel (d) shows the monthly median vertical chlorophyll profiles.

210 3.2 Temporal patterns in DCM presence, classification, and characteristics

DCMs were predominantly found in stratified water conditions (56.5 % of stratified profiles vs 3.3 % of mixed profiles; 3133/5543 vs 97/2943); thus, the seasonal presence of DCMs followed the seasonal pattern in water column stratification with peak presence from October until March (>64 %; Fig. 3b). However, despite stratification in at least 30 % of profiles in winter, DCMs practically disappeared in May–July (<3 % of profiles; Fig. 3b) changing the vertical chlorophyll distribution into a sigmoid shape (Fig. 3d). Overall, DCMs formed between the surface and 167.1 m deep, at a median depth of 75.3 m (IQR 29.3 m). However, median DCM depths varied seasonally with shallowing events in January (68.6 m; IQR 19.8 m), April (38.6 m; IQR 19.7 m), and September (65.4 m; IQR 38.4 m). Seasonal maxima depths were reached in February (75.2 m; IQR 32.3 m), July (95.9 m; IQR 130.8 m), and December (83.0 m; IQR 31.1 m), though DCMs in July appeared to either form close to the surface or at great depths (Fig. 4a). From June until December, there was an overall deepening trend during which the chlorophyll maximum moved further away from the mixed layer while remaining at an approximate constant relative distance from the euphotic zone (~1.1 times the euphotic zone depth; Fig. 4b). Median DCM half-peak widths concurrently narrowed (Fig. 4c), while the maximum chlorophyll concentration showed a modest increase (Fig. 4d). The exception to this trend was a brief shallowing to just above the bottom of the euphotic zone in September (0.99; IQR 0.45), characterised by a rapid increase in peak chlorophyll levels at the DCM. A contrasting shallowing trend can be discerned from December until April, positioning the chlorophyll maximum at a nearly constant relative distance from the bottom of the mixed layer (~2.0 times the mixed layer depth), but elevating the chlorophyll maximum to well within the euphotic zone in April (0.75; IQR 0.19). Despite this shallowing trend, DCMs remained of a similar width as in December and modest intensification of the chlorophyll maximum continued until a sudden deepening, widening, and weakening of the DCM in May.



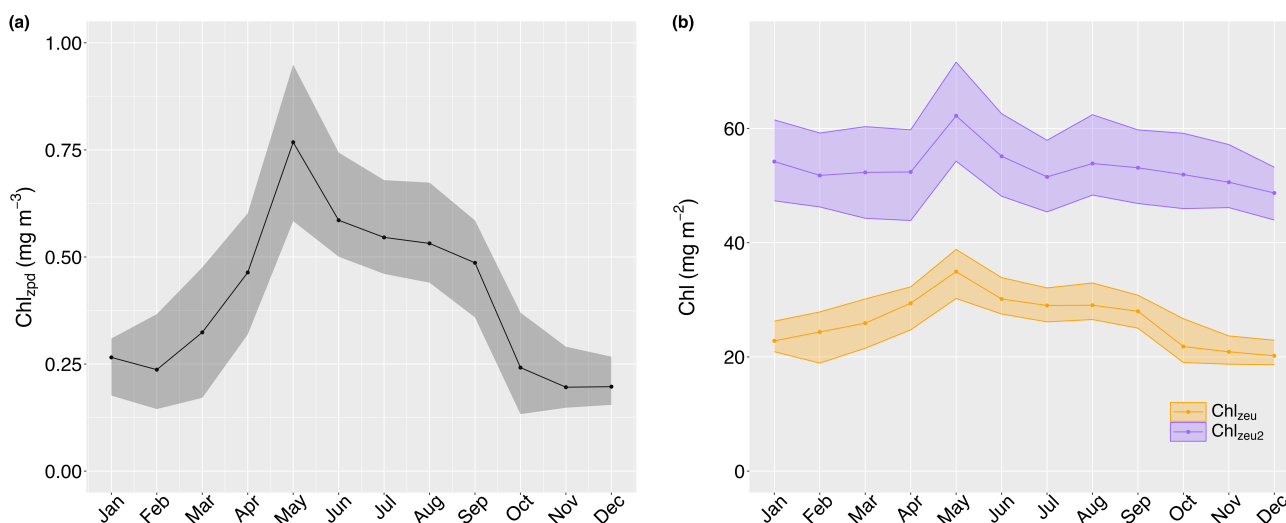
230 **Figure 4: Median monthly true DCM depth (Z_{dcm} ; panel a) and relative depth in relation to the bottom of the mixed layer ($Z_{\text{dcm}}/\text{MLD}$) and euphotic zone ($Z_{\text{dcm}}/Z_{\text{eu}}$; panel b). Panel (c) and (d) reflect the seasonal change in DCM width and maximum chlorophyll concentration at the DCM. Shaded ribbons in panel (b) and (c) indicate the 25th and 75th quartiles.**

Particle backscatter data were available for 1551 profiles, of which 95.8 % were collected in September–March (1487/1551). Over this time, the proportion of DBMs gradually declined from 69.7 % in September to 46.2 % in January, which is also

235 shown by a disproportional change in maximum particle backscatter and chlorophyll amplitudes (see Supplementary Fig. S4
for temporal patterns in DBM and DAM characteristics). As the DCM shallowed in late summer, DBMs became more
prevalent again with a peak presence in March (81 %). However, the sudden deepening, widening, and weakening of the DCM
in May pivoted DCM-type classifications to a prevalence of DAMs (70 %), which generally dominated in winter (i.e., 66.1
240 of the maximum chlorophyll relative to the euphotic zone depth remained within 1.2 times the euphotic zone depth.

3.3 Relationships between surface and water column-integrated chlorophyll

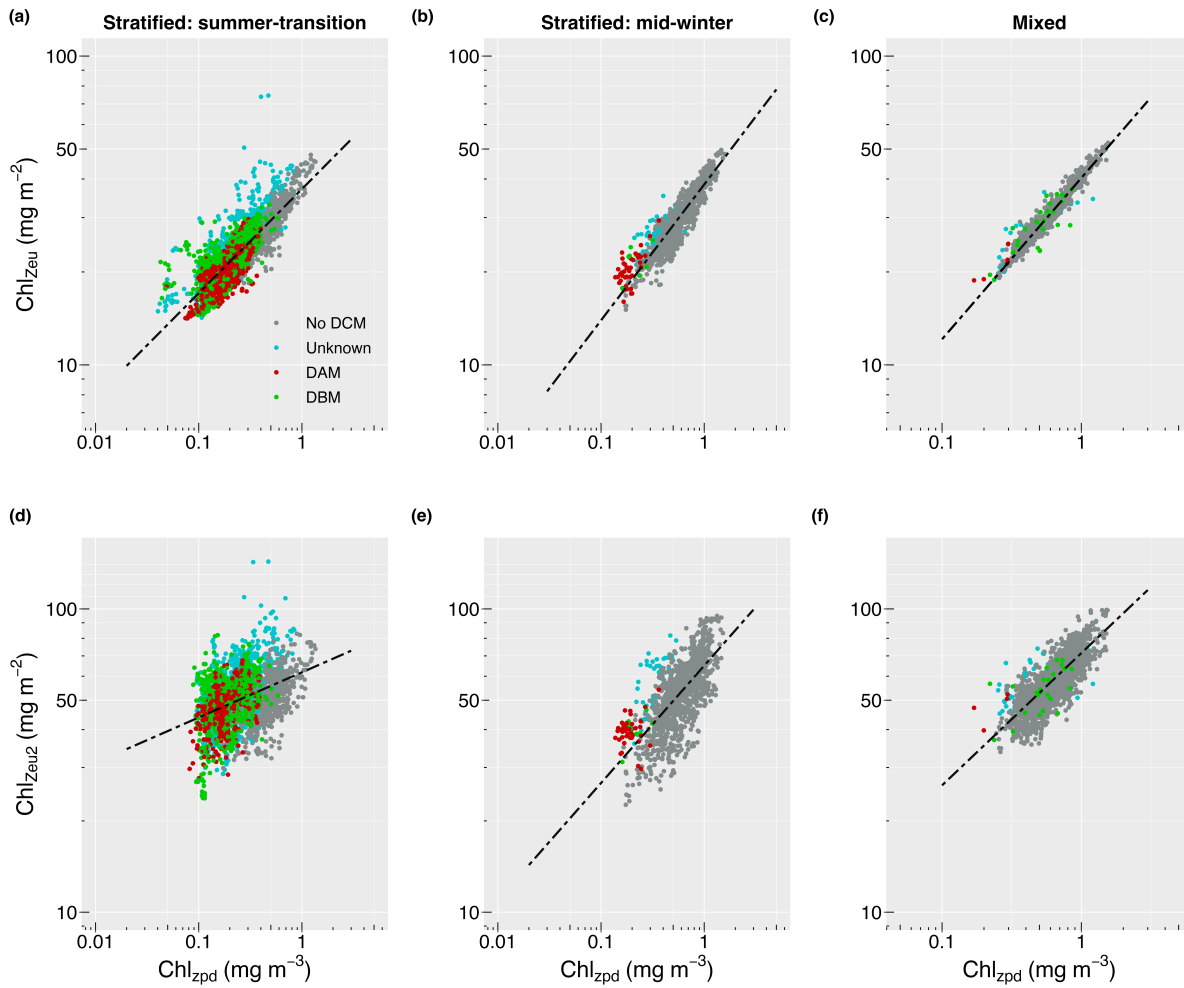
Surface chlorophyll concentrations (Chl_{zpd}) ranged between 0.04 and 1.58 $mg\ m^{-3}$ (median 0.44 $mg\ m^{-3}$, IQR 0.38 $mg\ m^{-3}$),
with marked seasonal changes (Fig. 5a). Monthly median surface chlorophyll values peaked in May (0.77 $mg\ m^{-3}$, IQR 0.37
 $mg\ m^{-3}$; Fig. 5a), remained $>0.5\ mg\ m^{-3}$ in winter, but rapidly decreased over September to minimum median levels $\sim 0.20\ mg\ m^{-3}$
245 m^{-3} in November and December. A subsequent increase can be discerned for January (0.27 $mg\ m^{-3}$, IQR 0.13 $mg\ m^{-3}$), though
values remained $<0.33\ mg\ m^{-3}$ throughout early autumn before rapidly transitioning to peak levels over April. A similar
seasonal pattern was present in depth-integrated chlorophyll values, albeit less pronounced (Chl_{zeu} ; Fig. 5b). Interestingly,
monthly median deep depth-integrated chlorophyll similarly peaked in May (Chl_{zeu2} ; 62.2 $mg\ m^{-2}$, IQR 17.3 $mg\ m^{-2}$) but a
secondary increase can be discerned in August (53.9 $mg\ m^{-2}$, IQR 14.1 $mg\ m^{-2}$), after which levels declined less rapidly to the
250 seasonal minimum in December (48.7 $mg\ m^{-2}$, IQR 9.2 $mg\ m^{-2}$; Fig. 5b). In January, deep-depth integrated chlorophyll
increased more evidently than depth-integrated values and subsequently remained relatively constant from February until April
(i.e., $\sim 52.0\ mg\ m^{-2}$). Overall, chlorophyll below the euphotic zone depth accounted for 50–60% of deep depth-integrated values
from October until March, declining to a minimum of 44 % in April, May, and July.



255

Figure 5: Monthly median surface (Chl_{zpd} ; panel a), depth-integrated (Chl_{zeu} ; orange solid line in panel b) and deep depth-integrated (Chl_{zeu2} ; purple solid line in panel b) chlorophyll values with their 25th and 75th quartiles as shaded areas.

Profiles collected from stratified water conditions in summer-transition months showed a significant linear relationship between surface and depth-integrated chlorophyll concentrations ($R^2 = 0.72$, $F_{(1,4002)} = 10420$, $p < 0.001$; Fig. 6a). A stronger relationship with a steeper slope and less scatter was seen for the stratified mid-winter months ($R^2 = 0.87$, $F_{(1,1533)} = 10080$, $p < 0.001$; Fig. 6b) and mixed water columns ($R^2 = 0.97$, $F_{(1,2940)} = 90400$, $p < 0.001$; Fig. 6c). Scatter around the regression line resulted from the presence of DCMs with no apparent difference between the contribution of DBMs and DAMs. Thus, the mean relative error was highest (8.9 %; MAE = 1.089) for estimates of observed depth-integrated chlorophyll from surface chlorophyll values under stratified water conditions in summer-transition months, when DCMs were more common. Under stratified water conditions in winter and mixed water conditions, the mean relative error reduced to 5.6 % and 1.7 %, respectively (i.e., MAE: 1.056 and 1.017, respectively). Scatter in the data increased for deep depth-integrated values, resulting in a weak linear relationship in stratified summer-transition months ($R^2 = 0.15$, $F_{(1,2729)} = 498.5$, $p < 0.001$; Fig. 6d) and a moderate relationship in both stratified mid-winter months ($R^2 = 0.48$, $F_{(1,1351)} = 1232$, $p < 0.001$; Fig. 6e) and mixed water columns ($R^2 = 0.63$, $F_{(1,2512)} = 4239$, $p < 0.001$; Fig. 6f). As a result, mean relative errors increased to 15.7 %, 15.2 %, and 8.6 %, respectively. All derived non-linear relationships are summarised in Table 2.



275 **Figure 6: Relationship between surface (Chl_{zpd}) and depth-integrated (Chl_{zeu}) vs. deep depth-integrated (Chl_{zeu2}) chlorophyll values for stratified water conditions in summer-transition months (i.e., September–April; a, d), stratified water conditions in mid-winter months (i.e., May–August; b, e), and mixed water conditions (c, f). Dots are coloured according to whether a DCM was absent (grey), present but of unknown type (turquoise), a DBM (green), or a DAM (dark red). Black dashed lines indicate the derived regression lines. Note the change in y-axis range between panels a–c and d–f and the change in x-axis range between stratified ($Z_{eu} > \text{MLD}$) and mixed water ($Z_{eu} < \text{MLD}$) conditions.**

280 **Table 2: Summary of non-linear relationships between surface (Chl_{zpd}) and depth-integrated (Chl_{zeu}) vs. deep depth-integrated (Chl_{zeu2}) chlorophyll under stratified and mixed water conditions. Relationships in stratified waters are given for both summer-transition (September–April) and mid-winter months (May–August).**

Water condition	Integration depth	Regression	R^2	MAE	Bias
<i>Stratified</i>					
Summer-Transition	Z_{eu}	$\text{Chl}_{zeu} = 37.1 \times \text{Chl}_{zpd}^{0.337}$	0.72	1.089	1.00

Mid-Winter	Z_{eu}	$Chl_{zeu} = 38.4 \times Chl_{zpd}^{0.440}$	0.87	1.056	1.00
Summer-Transition	Z_{eu2}	$Chl_{zeu2} = 61.8 \times Chl_{zpd}^{0.149}$	0.15	1.157	1.00
Mid-Winter	Z_{eu2}	$Chl_{zeu2} = 65.0 \times Chl_{zpd}^{0.387}$	0.48	1.152	1.00
<i>Mixed</i>					
Year-round	Z_{eu}	$Chl_{zeu} = 40.3 \times Chl_{zpd}^{0.522}$	0.97	1.017	1.00
Year-round	Z_{eu2}	$Chl_{zeu2} = 71.5 \times Chl_{zpd}^{0.436}$	0.63	1.086	1.00

4 Discussion

4.1. Seasonality in water column characteristics and DCM formation

The marine environment of Western Australia is governed by the warm poleward-flowing Leeuwin Current of tropical origin, with signatures from the higher salinity subtropical Indian central waters (Waite et al., 2007; Woo and Pattiaratchi, 2008). Because of generally low surface chlorophyll values beyond the continental shelf and a broad winter increase in surface chlorophyll from May until September, Western Australian waters are often labelled as oligotrophic (e.g., Twomey et al., 2007; Feng et al., 2009; Rennie et al., 2009a; Chen et al., 2019) with a surface productivity regime comparable to subtropical gyres (Koslow et al., 2008). These subtropical areas are characterised by either permanently stratified water columns or brief (~1 month) mixing periods, resulting in a (near) permanent DCM presence (Mignot et al., 2014; Quartly et al., 2023). Our results show that stratification in winter (May–August) is intermittent and that DCM formation is the exception rather than the norm (i.e., <3% of profiles). The disappearance of DCMs from vertical profiles corresponds to a period of intense Leeuwin Current strength, which is known to weaken stratification (i.e., May–July; Koslow et al., 2008; Feng et al., 2003, 2009). In addition, north-westerly down-welling favourable storms (wind speeds $>15 \text{ m s}^{-1}$; most frequent June–August) and concomitant surface cooling mix the water column down to 200 m depth, breaking down the stratified layer and DCM (Rennie et al., 2006; Chen et al., 2020). While re-stratification has been shown to occur during subsequently calm post-storm south-westerly winds (wind speeds $<7 \text{ m s}^{-1}$; Rennie et al., 2006), our data reveal that these re-stratification periods often do not persist long enough for DCMs to reform. This is likely because of the additive effect of increased eddy kinetic energy, which peaks in July (Feng et al., 2005). Warm-core eddies, in particular, are frequent in late autumn and winter between 28° and 31° S, generating well-mixed layers extending beyond the euphotic zone depth (Thompson et al., 2007; Waite et al., 2007). Consequently, our area experiences a mixing period of approximately three months, which is more comparable to the duration of mixing periods in the Mediterranean (Mignot et al., 2014; Barbieux et al., 2019) and oligotrophic sub-tropical open oceans (Chiswell et al., 2022).

4.2. DCM characteristics

305 Leeuwin Current strength significantly drops (Feng et al., 2003) and winter storms settle in September (Pearce et al., 2015), which is when stratified water columns return. However, eddy kinetic energy remains persistent (Feng et al., 2009). Warm-core eddies have been hypothesised to allow late winter/early autumn phytoplankton blooms through the injection of nitrogen into surface waters (Lourey et al., 2013) and the formation of a shallow nutricline (~60 m depth) under a relaxed Leeuwin Current after eddies detach from the shelf (Koslow et al., 2008). Our data supports this hypothesis with a reappearance of

310 DCMs in September at a median depth of 65.4 m, which were predominantly biomass maxima. The subsequently observed deepening of the DCM through spring and summer is common for oligotrophic regions (Mignot et al., 2014; Chiswell et al., 2022). In our study area, as the DCM deepened and intensified, backscatter vertical profiles changed disproportional to chlorophyll vertical profiles, reflecting the decreased occurrence of DBMs until biomass and photo-acclimation maxima occurred in approximately equal proportions from December until February. DCM formation is always at least in part caused

315 by photo-acclimation of phytoplankton to low light conditions (Cullen, 2015) but deep DCMs in summer may approach the nutricline, allowing for phytoplankton growth and thus, DBM formation (Mignot et al., 2014). DCM settlement within a nearly constant distance from the euphotic zone depth (i.e., ~1.1 times the euphotic zone depth), regardless of DCM type, suggests photo-acclimation processes in response to light limitation as the main driver of DCM formation from September until late summer. However, the balanced presence of photo-acclimation and biomass maxima in our study indicates that access to

320 nutrients is indeed available throughout summer. These findings fit the equal occurrence of upwelling and downwelling days detected in temperature time series by Rennie et al. (2006) and positioning of the summer DCM just above the nutricline in earlier studies (e.g., Hanson et al., 2007a, 2007b; Koslow et al., 2008). In addition, Rennie et al., (2006) detected a concentration of upwelling events in late February–early March, which temporally matches with an initial weakening of stratification as the Leeuwin Current starts to intensify (Feng et al., 2003; Koslow et al., 2008) and in our study, with the timing

325 of DCM shallowing, intensification, and a rapid increase in biomass maxima. Thus, while the DCM formation is first-order light-driven, nutrient limitation in the upper water column in autumn and at depth in summer likely drives the balance between biomass and photo-acclimation maxima until upwelling and increased water turbidity potentially synergistically increase nutrient levels within the bottom layer of the euphotic zone. Our results suggest that DCMs in Western Australian waters form via bio-optical mechanisms that match neither pattern observed in subtropical oceanic (Mignot et al., 2014; Chiswell et al.,

330 2022; Quartly et al., 2023) and more productive temperate regions (Mignot et al., 2014; Barbieux et al., 2019), but instead are similar to the mid-Mediterranean Sea, which forms a transition between the meso-oligotrophic western and oligotrophic eastern basins (Barbieux et al., 2019). However, a broad-scale long-term study, including nutrient and irradiance parameters, is required to elucidate our hypothesis.

4.3. Water column-integrated productivity

335 Seasonal surface chlorophyll fluctuations followed the commonly observed pattern of a winter surface chlorophyll increase, albeit our observed peak in May proceeding the June–July winter bloom previously described by Lourey et al. (2006) and Koslow et al. (2008). This shift could be related to changing trends in environmental and oceanographic drivers. Long-term data series from IMOS national reference stations around Australia have shown, for example, that mixed layer and euphotic zone depth follow an overall deepening trend from 2008 to 2018 by 1.02 m yr^{-1} and 1.7 m yr^{-1} , respectively (van Ruth et al., 340 2020). The seasonal pattern in depth-integrated chlorophyll levels showed a flatter annual cycle but remained largely similar in shape. This flattening originates from the inclusion of DCMs in depth-integrated values in summer. Since DCMs predominantly formed below our defined euphotic zone depth, contributing $>50 \%$ to water column integrated values in summer, the seasonal cycle diminished even further when integrating over twice the euphotic zone depth (i.e., deep depth-integrated chlorophyll). Interestingly, deep-depth integrated values showed chlorophyll increases in May, August, and January, 345 which correspond to previously identified temporal peaks in water-column integrated net primary productivity (Koslow et al., 2008), albeit again with an apparent one-month advance. These findings support our hypothesis that deep-depth integrated values may be a better predictor variable to include in marine animal habitat models for ocean regions where DCMs are present. However, there are currently no means to include water column-integrated chlorophyll levels in habitat models that aim to relate large spatiotemporal animal presence data sets with environmental variables such as chlorophyll. While ocean glider 350 and biogeochemical-Argo float datasets have greatly advanced our ability to study subsurface biogeochemical processes, the spatiotemporal extent of these data often does not align with animal presence data from land-based, boat-based, and underwater acoustic platforms. It is, therefore, pivotal to develop our knowledge of potential methods that facilitate depth-integrated chlorophyll estimates from openly available data sources, such as satellite remote sensing.

The lack of existing methods and presence of a DCM with potential importance to migrating locally endangered pygmy blue 355 whales was the main driving factor for us to assess whether known relationships between surface and depth-integrated chlorophyll in open ocean and mesotrophic regions (Morel and Berthon, 1989; Uitz et al., 2006; Frolov et al., 2012), were also present in the unique marine environment of Western Australia. Our results confirm that similar relationships are present within the nutrient-deprived western boundary current system of Western Australia, albeit with a replacement of the traditional two-part regression line for stratified water columns with a seasonally dependent regression line. This seasonal change reflects 360 the seasonal patterns in water stratification and DCM formation. Low surface chlorophyll levels and deeper DCMs characterised the stratified water column in summer-transition months, while alternating periods of increased winter mixing and weak re-stratifications from May until August predominantly break down the DCM. Graff and Behrenfeld (2018) found that deep water entrainment followed by re-stratification in the North Atlantic rapidly increased surface chlorophyll (and phytoplankton biomass) over three days post-entrainment event, while chlorophyll decreased at a much slower rate at depth. 365 Hence, changes in surface chlorophyll contributed more strongly to changing depth-integrated values. The sigmoid vertical chlorophyll profiles in winter suggest that similar processes may be at play during calm winter periods in our study area,

accounting for the steeper slope derived from stratified water profiles in mid-winter (i.e., 0.440). The strong relationship with an even steeper slope (0.522; $R^2 = 0.97$) and little error in mixed water conditions reflect the even more extensive homogenous vertical distribution of chlorophyll present under these conditions (Morel and Berthon, 1989; Uitz et al., 2006). Extending
370 chlorophyll integrations to twice the euphotic zone depth showed similar functional relationships, albeit with a higher MAE, especially in summer-transition months. Scatter in the data at low surface chlorophyll values was predominantly attributable to the inclusion of full DCM widths in deep depth-integrated values, confirming earlier statements by Morel and Berthon (1989) and Uitz et al., (2006). However, despite the increased scatter, the MAEs for relationships over twice the euphotic zone depth remained low for all three conditions (i.e., 16.3 %, 15.7 %, and 8.6 %).

375 **4.4. From water column-integrated chlorophyll estimates to whales**

Potential links between the physical oceanography, biogeochemical processes, and pygmy blue whale presence in the Perth Canyon have been studied previously (Rennie, 2005). Based on numerical models (Rennie et al., 2009b), moored temperature time series analyses (Rennie et al., 2006), and in situ data collection during oceanic cruises (Rennie et al., 2009a), Rennie and co-authors hypothesised that winter productivity supports the local krill population through spring with sporadic summer
380 upwelling events allowing krill to grow to an appropriate size for whale consumption from February onward (Rennie et al., 2009a). Indeed, food availability is a crucial driver of Euphausiid health (i.e., lipid content; Fisher et al., 2020; Hellessey et al., 2020; Steinke et al., 2021), timing of reproduction (Quentin and Ross, 2001; Schmidt et al., 2012), hatching success (Yoshida et al., 2011; Steinke et al., 2021), and growth rate (Bahlburg et al., 2023). Thus, a regular supply of phytoplankton prey seems crucial for population maintenance. In addition, baleen whales show a preference for krill >16 mm (Croll et al.,
385 2005; Cade et al., 2022). Consequently, peak abundances of foraging baleen whales reportedly lag the onset or peak intensity of phytoplankton blooms by 1–4 months (Croll et al., 2005; Visser et al., 2010). In the absence of a defined sub-surface chlorophyll bloom and instead a consistent balanced presence of photo-acclimation and biomass maxima, we believe that our results are in support of continuous krill population maintenance through DCM formation in summer. However, rather than the winter surface bloom, we suggest that an increase in productivity at the DCM around September (i.e., early spring) sets the
390 scene for krill maintenance through summer and a sufficient prey abundance for arriving foraging pygmy blue whales ~4 months later. In addition, the sudden increased presence of biomass maxima in March may be a crucial feature in support of pygmy blue whale foraging efforts throughout autumn and early winter or alternatively, support a new spawning event (e.g., Paul et al., 1990; Feinberg and Peterson, 2003; Plourde et al., 2011).

4.5. Future habitat models and potential pitfalls

395 Based on our results and in the absence of other means to include high spatiotemporal resolution subsurface chlorophyll data, we encourage the use of water column-integrated chlorophyll (over twice the euphotic zone depth) estimates from satellite remote sensing in future marine animal habitat models. Of course, we acknowledge challenges related to potential regression

biases and the translation from fluorescence-derived relationships to satellite-derived estimates. Besides scatter in the regression line being caused by DCM presence, there are other sources of potential bias that deserve further investigation. For instance, we may have introduced additional scatter in our regression lines with our definition of the euphotic zone depth as $Z_{1\%}^{\text{PAR}}$ and simple extension to “twice the euphotic zone depth”. At low- and mid-latitudes specifically, $Z_{1\%}^{\text{PAR}}$ likely underestimates the compensation depth and so, $Z_{0.5\%}^{\text{PAR}}$, $Z_{0.9\%}^{\text{USR}}$ (i.e., depth at which 0.9 % of surface solar radiation is available; 400–560 nm), or $Z_{1.5\%}^{490}$ (i.e., depth at which 1.5 % of surface downwelling irradiance is available; 490 nm) have been suggested as more robust alternatives (Wu et al., 2021). Euphotic zone depth estimates based on these alternative definitions do not vary in lockstep with those based on $Z_{1\%}^{\text{PAR}}$ (Wu et al., 2021), so using a more appropriate definition of the euphotic zone may decrease the scatter observed. In addition, and more of a general concern, Roesler et al. (2017) recently found that factory-calibrated chlorophyll concentrations, as estimated by WET Labs ECO optical sensors used in our study, overestimate measured chlorophyll on average by a factor of 2. While a study on the northwest Western Australian shelf, which has a similar phytoplankton community as found in the Perth Canyon, showed good agreement between chlorophyll concentrations from optical sensors and HPLC-derived chlorophyll from simultaneously collected water samples ($R^2 = 0.75$, slope factor = 1.2; Thomson et al., 2015), we highlight the need for a similar comparative study in any area of interest. These sources of uncertainty come on top of the well-known inconsistency in chlorophyll to carbon ratio related to changing phytoplankton communities and environmental effects other than photo-acclimation (Cullen, 1982).

It is also worth noting that the data set used in this study provided insufficient consistent spatial and temporal coverage, with some years (e.g., 2008, 2019, and 2020) and some months (e.g., January, April, and October) sampled considerably less than others (see Supplementary Fig. S1). This was especially true for particle backscatter coefficient data. Inconsistencies in spatial and temporal replication make seasonal analyses less robust and prohibit the elucidation of potential environmental effects on seasonal patterns. Inter-annual variation in productivity within the Western Australian marine environment is primarily related to fluctuations in the Leeuwin Current strength following the El Niño Southern Oscillation (ENSO; Feng et al., 2009; Chen et al., 2019). Three strong ENSO events occurred during the study period (i.e., one El Niño and two La Niña’s; Australian Bureau of Meteorology, 2023), and we recommend that their effects on the robustness of seasonal patterns in DCM formation and characteristics as well as linear relationships found are further assessed. Such assessments will require dedicated data collection, preferably within areas of biological interest to marine animals.

5 Conclusion

To our best available knowledge, this is the first study to classify the productivity biome of Western Australian marine waters as an intermediate version of subtropical and temperate (meso) oligotrophic areas, highlighting the concealing nature of traditional biogeographical classifications (Bock et al., 2022). Our results provide evidence of phytoplankton biomass increases in early spring and autumn, which, together with a consistently balanced presence of photo-acclimation and biomass maxima in summer, likely support the local krill population sufficiently enough to be of relevance to foraging pygmy blue whales. Our

430 results highlight the potential and need to monitor deep depth-integrated primary productivity patterns via satellite remote sensing in regions where DCMs occur, which can be achieved through water-column integrated chlorophyll estimates from surface chlorophyll values. We suggest including satellite-derived deep depth-integrated chlorophyll estimates (i.e., integrations over twice the euphotic zone depth) in future efforts to identify productivity hotspots and anomalies off Western Australia in an attempt help better understand the occurrence and behaviour of marine animal species, such as pygmy blue
435 whales. Similar methods can be applied to other (intermittent) oligotrophic areas where DCMs may be an important feature for higher trophic levels. However, while our regression line slopes for the euphotic zone closely resemble those previously obtained from stratified (range 0.310–0.425 for $\text{Chl}_{zpd} < 1 \text{ mg m}^{-3}$; Morel and Berthon, 1989; Uitz et al., 2006; Frolov et al., 2012) and mixed water samples (0.551 and 0.538; Morel and Berthon, 1989; Uitz et al., 2006), it is clear that regression parameters need to be locally tuned and that sources of potential estimate biases need to be further explored.

440 **Data availability**

All raw ocean glider data (i.e., IMOS – Australian National Facility for Ocean Gliders (ANFOG) – delayed mode glider deployments), subsetted to the spatial extent in this manuscript, are openly available from the Australian Ocean Data Network portal at <https://portal.aodn.org.au/>. The extracted vertical profiles used for data analysis in this study are available from the corresponding author upon request.

445 **Author contributions**

Author Contributions: RPS: Conceptualisation, methodology, coding, data acquisition & analysis, visualisation, original draft preparation, reviewing & editing; CE: Conceptualisation (supporting), supervision, reviewing & editing; RDM: Conceptualisation (supporting), supervision, reviewing & editing.

Competing interests

450 The authors declare that they have no conflict of interest.

Financial support

We acknowledge the Australian Government's support through an Australian Government Research Training Program Scholarship awarded to RPS.

Acknowledgements

455 We would like to acknowledge the Integrated Marine Observing System’s Australian National Facility for Ocean Gliders (IMOS-ANFOG), from which ocean glider data used in this study was sourced. IMOS is enabled by the National Collaborative Research Infrastructure Strategy (NCRIS) and is operated by a consortium of institutions as an unincorporated joint venture, with the University of Tasmania as a lead agent. Credit should also be given to the University of Western Australia (UWA) as the operating institution of ANFOG. Thanks to David Antoine for reading through the final draft and providing meaningful
460 feedback throughout the development of this manuscript. Finally, thanks to two anonymous reviewers for their invaluable comments to help improve this manuscript.

References

- Australian Bureau of Meteorology: Climate driver update: Climate drivers in the Pacific, Indian and Southern Oceans and the tropics, last accessed October 11, 2023: <http://www.bom.gov.au/climate/enso/#tabs=Indian-Ocean>, 2023.
- 465 Bahlburg, D., Thorpe, S. E., Meyer, B., Berger, U., and Murphy, E. J.: An intercomparison of models predicting growth of Antarctic krill (*Euphausia superba*): The importance of recognizing model specificity, PLoS One, 18, e0286036, <https://doi.org/10.1371/journal.pone.0286036>, 2023.
- Baldry, K., Strutton, P. G., Hill, N. A., and Boyd, P. W.: Subsurface chlorophyll-a maxima in the Southern Ocean, Front Mar Sci, 7, 671, <https://doi.org/10.3389/fmars.2020.00671>
- 470 Barbieux, M., Uitz, L., Gentili, B., de Fommervault, O. P., Mignot, A., Poteau A., Schmechtig, C., Taillandier, V., Leymarie, E., Penkerch, C., D’Ortenzio, F., Claustre, H., and Bricaud, A.: Bio-optical characterization of subsurface chlorophyll maxima in the Mediterranean Sea from a biogeochemical-Argo float database, Biogeosciences, 16, 1321–1342, <https://doi.org/10.5194/bg-16-1321-2019>, 2019.
- Bock, N., Cornec, M., Claustre, H., and Duhamel, S.: Biogeographical classification from the global ocean from BGC-Argo
475 floats, Global Biogeochem Sci, 36, e2021GB007233, <https://doi.org/10.1029/2021GB007233>
- Boettger, D., Robertson, R., and Brassington, G. B.: Verification of the mixed layer depth in the OceanMAPS operational forecast model for Austral autumn, Geosci Model Dev, 11, 3795–3805, <https://doi.org/10.5194/gmd-11-3795-2018>, 2018.
- de Boyer Montégut, C., Madec, G., Fischer, A. S., Lazar, A., and Iudicone, D.: Mixed layer depth over the global ocean: An examination of profile data and a profile-based climatology, J Geophys Res Oceans, 109, C12003,
480 <https://doi.org/10.1029/2004JC002378>, 2004.
- Cade, D. E., Kahane-Rapport, S. R., Wallis, B., Goldbogen, J. A., and Friedlaender, A. S.: Evidence for size-selective predation by Antarctic humpback whales, Front Mar Sci, 9, 747788, <https://doi.org/10.3389/fmars.2022.747788>, 2022.
- Chai, T. and Draxler, R. R.: Root mean square error (RMSE) or mean absolute error (MAE)? — Arguments against avoiding RMSE in the literature, Geosci Model Dev, 7, 1247–1250, <https://doi.org/10.5194/gmd-7-1247-2014>, 2014.

- 485 Chen, M., Pattiaratchi, C. B., Ghadouani, A., and Hanson, C.: Seasonal and inter-annual variability of water column properties along the Rottneest continental shelf, south-west Australia, *Ocean Sci*, 15, 333–348, <https://doi.org/10.5194/os-15-333-2019>, 2019.
- Chen, M., Pattiaratchi, C. B., Ghadouani, A., and Hanson, C.: Influence of storm events on chlorophyll distribution along the oligotrophic continental shelf off south-western Australia, *Front Mar Sci*, 7, 287, <https://doi.org/10.3389/fmars.2020.00287>,
490 2020.
- Chiswell, S. M., Gutiérrez-Rodríguez, A., Gall, M., Safi, K., Strzepak, R., Décima, M. R., Nodder, S. D.: Seasonal cycles of phytoplankton and net primary production from Biogeochemical Argo float data in the south-west Pacific Ocean, *Deep Sea Res Pt I*, 187, 103834, <https://doi.org/10.1016/j.dsr.2022.103834>, 2022
- Cornec, M., Claustre, H., Mignot, A., Guidi, L., Lacour, L., Poteau, A., D’Ortenzio, F., Gentili, B., and Schmechtig, C.: Deep
495 chlorophyll maxima in the global ocean: Occurrences, drivers and characteristics, *Global Biogeochem Cycles*, 35, e2020GB006759, <https://doi.org/10.1029/2020GB006759>, 2021.
- Cresswell, G. R., and Golding, T. J.: Observations of a south-flowing current in the southeastern Indian Ocean, *Deep Sea Res Pt A Oceanogr Res Papers*, 27, 449–466, [https://doi.org/10.1016/0198-0149\(80\)90055-2](https://doi.org/10.1016/0198-0149(80)90055-2), 1980.
- Croll, D. A., Marinovic, B., Benson, S., Chavez, F. P., Black, N., Ternullo, R., and Tershly, B. R.: From wind to whales:
500 Trophic links in a coastal upwelling system, *Mar Ecol Prog Ser*, 289, 117–130, <https://doi.org/10.3354/MEPS289117>, 2005.
- Cullen, J. J.: The deep chlorophyll maximum: Comparing vertical profiles of chlorophyll a, *Can J Fish Aquat Sci*, 39, 791–803, <https://doi.org/10.1139/f82-108>, 1982.
- Cullen, J. J.: Subsurface chlorophyll maximum layers: Enduring enigma or mystery solved?, *Ann Rev Mar Sci*, 7, 207–239, <https://doi.org/10.1146/annurev-marine-010213-135111>, 2015.
- 505 Double, M. C., Andrews-Goff, V., Jenner, K. C. S., Jenner, M. N., Laverick, S. M., Branch, T. A., and Gales, N. J.: Migratory movements of pygmy blue whales (*Balaenoptera musculus brevicauda*) between Australia and Indonesia as revealed by satellite telemetry, *PLoS One*, 9, e95378, <https://doi.org/10.1371/journal.pone.0093578>, 2014.
- Erbe, C., Verma, A., McCauley, R., Gavrilov A., and Parnum I.: The marine soundscape of the Perth Canyon, *Prog Oceanogr*, 137, 38–51, <https://doi.org/10.1016/j.pocean.2015.05.015>, 2015.
- 510 Fearn, P. R., Twomey, L., Zakiyah, U., Hellenen, S., Vincent, W., and Lynch, M. J.: The Hillarys transect (3): Optical and chlorophyll relationships across the continental shelf off Perth, *Cont Shelf Res*, 27, 1719–1746, <https://doi.org/10.1016/j.csr.2007.02.004>, 2007.
- Feinberg, L. R. and Peterson, W. T.: Variability in duration and intensity of euphausiid spawning off central Oregon, 1996–2001, *Prog Oceanogr*, 57, 363–379, [https://doi.org/10.1016/s0079-6611\(03\)00106-X](https://doi.org/10.1016/s0079-6611(03)00106-X), 2003.
- 515 Feng, M., Meyers, G., Pearce, A., Wijffels, S.: Annual and interannual variation of the Leeuwin Current at 32°S, *J Geophys Res*, 108, 3355, <https://doi.org/10.1029/2002JC001763>, 2003
- Feng, M., Waite, A. M., and Thompson, P. A.: Climate variability and ocean production in the Leeuwin Current system off the west coast of Western Australia, *J R Soc West Aust*, 92, 67–81, 2009.

- 520 Fernand, L., Weston, K., Morris, T., Greenwood, N., Brown, J., and Jickells, T.: The contribution of the deep chlorophyll maximum to primary production in a seasonally stratified shelf sea, the North Sea, *Biogeochemistry*, 113, 153–166, <https://doi.org/10.1007/s10533-013-9831-7>, 2013.
- Fisher, J. L., Menkel, J., Copeman, L., Shaw, C. T., Feinberg, L. R., and Peterson, W. T.: Comparison of condition metrics and lipid content between *Euphausia pacifica* and *Thysanoessa spinifera* in the northern California Current, USA, *Prog Oceanogr*, 188, 102417, <https://doi.org/10.1016/j.pocean.2020.102417>, 2020.
- 525 Frolov, S., Ryan, J. P., and Chavez, F. P.: Predicting euphotic-depth-integrated chlorophyll-*a* from discrete-depth and satellite-observable chlorophyll-*a* off central California, *J Geophys Res Oceans*, 117, C05042, <https://doi.org/10.1029/2011JC007322>, 2012.
- Gieskes, W. W. C. and Kraay, G. W.: Continuous plankton records: Changes in the plankton of the North Sea and its eutrophic southern bight from 1948 to 1975, *Netherlands Journal of Sea Research*, 11, 334–364, [https://doi.org/10.1016/0077-7579\(77\)90014-X](https://doi.org/10.1016/0077-7579(77)90014-X), 1977.
- 530 Gordon, H. R. and McCluney, W. R.: Estimation of the depth of sunlight penetration in the sea for remote sensing, *Appl Opt*, 14, 413–416, <https://doi.org/10.1364/AO.14.000413>, 1975.
- Graff, J. R. and Behrenfeld, M. J.: Photoacclimation responses in subarctic Atlantic phytoplankton following a natural mixing-restratification event, *Front Mar Sci*, 5, 209, <https://doi.org/10.3389/fmars.2018.00209>, 2018.
- 535 Groom, S., Sathyendranath, S., Ban, Y., Bernard, S., Brewin, R., Brotas, V., Brockmann, C., Chauhan, P., Choi, J. K., Chuprin, A., Ciavatta, S., Cipollini, P., Donlon, C., Franz, B., He, X., Hirata, T., Jackson, T., Kampel, M., Krasemann, H., Lavender, S., Pardo-Martinez, S., Mélin, F., Platt, T., Santoleri, R., Skakala, J., Schaeffer, B., Smith, M., Steinmetz, F., Valente, A., and Wang, M.: Satellite ocean colour: Current status and future perspective, *Front Mar Sci*, 6, 485, <https://doi.org/10.3389/fmars.2019.00485>, 2019.
- 540 Hanson, C. E., Pattiaratchi, C. B., and Waite, A. M.: Seasonal production regimes off south-western Australia: Influence of the Capes and Leeuwin currents on phytoplankton dynamics, *Mar Freshw Res*, 56, 1011–1026, <https://doi.org/10.1071/MF04288>, 2005b.
- Hanson, C. E., Pattiaratchi, C. B., and Waite, A. M.: Sporadic upwelling on a downwelling coast: Phytoplankton responses to spatially variable nutrient dynamics off the Gascoyne region of Western Australia, *Cont Shelf Res*, 25, 1561–1582, <https://doi.org/10.1016/j.csr.2005.04.003>, 2005a.
- 545 Hanson, C. E., Pesant, S., Waite, A. M., and Pattiaratchi, C. B.: Assessing the magnitude and significance of deep chlorophyll maxima of the coastal eastern Indian Ocean, *Deep Sea Res 2 Top Stud Oceanogr*, 54, 884–901, <https://doi.org/10.1016/j.dsr2.2006.08.021>, 2007a.
- Hanson, C. E., Waite, A. M., Thomppson, P. A., and Pattiaratchi, C. B.: Plankton community structure and nitrogen nutrition in Leeuwin Current and coastal waters off the Gascoyne region of Western Australia, *Deep Sea Res Pt II*, 54, 902–924, <https://doi.org/10.1016/j.dsr2.2006.10.002>, 2007b.
- 550

- Hellessey, N., Johnson, R., Ericson, J. A., Nichols, P. D., Kawaguchi, S., Nicol, S., Hoem, N., and Virtue, P.: Antarctic krill lipid and fatty acid content variability is associated to satellite derived chlorophyll *a* and sea surface temperatures, *Sci Rep*, 10, 6060, <https://doi.org/10.1038/s41598-020-62800-7>, 2020.
- 555 Hobday, A. J. and Hartog, J. R.: Derived ocean features for dynamic ocean management, *Oceanography*, 27, 134–145, <https://doi.org/10.5670/oceanog.2014.92>, 2014.
- Hodson, T. O.: Root-mean-square error (RMSE) or mean absolute error (MAE): When to use them or not, *Geosci Model Dev*, 15, 5481–5487, <https://doi.org/10.5194/gmd-15-5481-2022>, 2022.
- Hovis, W. A., Clark, D. K., Anderson, F., Austin, R. W., Wilson, W. H., Baker, E. T., Ball, D., Gordon, H. R., Mueller, J. L.,
560 El-Sayed, S. Z., Sturm, B., Wrigley, R. C., and Yentsch, C. S.: Nimbus-7 coastal zone color scanner: System description and initial imagery, *Science* (1979), 210, 60–63, <https://doi.org/10.1126/science.210.4465.60>, 1980.
- Huot, Y., Babin, M., Bruyant, F., Grob, C., Twardowski, M. S., and Claustre, H.: Does chlorophyll *a* provide the best index of phytoplankton biomass for primary productivity studies?, *Biogeosciences Discussions*, 4, 707–745, <https://doi.org/10.5194/bg-4-853-2007>, 2007.
- 565 IMOS: IMOS - Australian Facility for Ocean Gliders (ANFOG) — delayed mode glider deployments, last accessed July 26, 2023: <https://portal.aodn.org.au>, 2023.
- IOC, SCOR, and IAPSO: The international thermodynamic equation of seawater - 2010: Calculation and use of thermodynamic properties, Intergovernmental Oceanographic Commission, Manuals and Guides, UNESCO, Paris, France, last accessed August 4, 2023: https://www.teos-10.org/pubs/TEOS-10_Manual.pdf, 2010.
- 570 Jeffrey, S. W.: Profiles of photosynthetic pigments in the Ocean using thin-layer chromatography, *Mar Biol*, 26, 101–110, <https://doi.org/10.1007/BF00388879>, 1974.
- Jeffrey, S. W., Wright, S. W., and Zapata, M.: Recent advances in HPLC pigment analysis of phytoplankton, *Mar Freshw Res*, 50, 879–896, <https://doi.org/10.1071/MF99109>, 1999.
- Koslow, J. A., Pesant, S., Feng, M., Pearce, A., Fearn, P., Moore, T., Matear, R., and Waite, A.: The effect of the Leeuwin
575 current on phytoplankton biomass and production off southwestern Australia, *J Geophys Res Oceans*, 113, C07050, <https://doi.org/10.1029/2007JC004102>, 2008.
- Lourey, M. J., Dunn, J. R., and Waring, J.: A mixed-layer nutrient climatology of Leeuwin current and Western Australian shelf waters: Seasonal nutrient dynamics and biomass, *Journal of Marine Systems*, 59, 25–51, <https://doi.org/10.1016/j.jmarsys.2005.10.001>, 2006.
- 580 Lourey, M. J., Thompson, P. A., McLaughlin, M. J., Bonham, P., and Feng, M.: Primary production and phytoplankton community structure during a winter shelf-scale phytoplankton bloom off Western Australia, *Mar Biol*, 160, 355–369, <https://doi.org/10.1007/s00227-012-2093-4>, 2013
- Mantovanelli, A., and Thomson, P. G.: Particle backscattering coefficient for Wetlab Ecopucks in IMOS ANFOG gliders, IMOS Technical Report, <https://doi.org/10.13130/RG.2.1.4875.5440>, 2016.

- 585 Marañón, E., Van Wambeke, F., Uitz, J., Boss, E. S., Dimier, C., Dinasquet, J., Engel, A., Haëntjens, N., Pérez-Lorenzo, M.,
Taillandier, V., and Zäncker, B.: Deep maxima of phytoplankton biomass, primary production and bacterial production in the
Mediterranean Sea, *Biogeosciences*, 18, 1749–1767, <https://doi.org/10.5194/bg-18-1749-2021>, 2021.
- McCauley, R. D., and Cato, D. H.: Evening choruses in the Perth Canyon and their potential link with Myctophidae fishes, *J
Acoust Soc Am* ,140, 2384–2398, <https://doi.org/10.1121/1.4964108>, 2014.
- 590 McCauley, R., Bannister, J. L., Burton, C. L. K. , et al Western Australian exercise area blue whale project. Final Summary
Report. Centre for Marine Science and Technology (CMST), Perth, Australia, Centre for Marine Science and Technology, 1-
73 pp., last accessed November 1, 2024: <http://cmst.curtin.edu.au/wp-content/uploads/sites/4/2016/05/2004-29.pdf>, 2004.
- McClain, C. R.: Satellite remote sensing: Ocean color, in: *Encyclopedia of Ocean Sciences*, edited by: Steele, J. H., Academic
Press, San Diego, CA, United States, 114–126, 2009.
- 595 McDougall, T. J. and Barker, P. M.: Getting started with TEOS-10 and the Gibbs Seawater (GSW) Oceanographic Toolbox
version 3.06.12, SCOR/IAPSO, 1–28 pp., last accessed August 4, 2023: https://www.teos-10.org/pubs/Getting_Started.pdf,
2020.
- Mignot, A., Claustre, H., Uitz, J., Poteau, A., D’Ortenzio, F., and Xing, X.: Understanding the seasonal dynamics of
phytoplankton biomass and the deep chlorophyll maximum in oligotrophic environments: A bio-argo float investigation,
600 *Global Biogeochem Cycles*, 28, 856–876, <https://doi.org/10.1002/2013GB004781>, 2014.
- Morel, A. and Berthon, J. F.: Surface pigments, algal biomass profiles, and potential production of the euphotic layer:
Relationships reinvestigated in view of remote-sensing applications, *Limnol Oceanogr*, 34, 1545–1562,
<https://doi.org/10.4319/lo.1989.34.8.1545>, 1989.
- Morel, A. and Maritorena, S.: Bio-optical properties of oceanic waters: A reappraisal, *J Geophys Res Oceans*, 106, 7163–
605 7180, <https://doi.org/10.1029/2000jc000319>, 2001.
- Organelli, E., Barbieux, M., Claustre, H., Schmechtig, C., Poteau, A., Bricaud, A., Boss, E., Briggs, E., Dall’Olmo, G.,
D’Ortenzio, F., Leymarle, E., Mangin, A., Obolensky, G., Penkerch, C., Prieur, L., Roesler, C., Serra, R., Uitz, J., and Xing,
X.: Two databases derived from BGC-Argo float measurements for marine biogeochemical and bio-optical applications, *Earth
Syst Sci Data*, 9, 861-880, <https://doi.org/10.5194/essd-9-861-2017>, 2017.
- 610 Owen, K., Jenner, C. S., Jenner, M.-N. M., and Andrews, R. D. : A week in the life of a pygmy blue whale: Migratory dive
depth overlaps with large vessel drafts, *Anim Biotelemetry*, 4, 17, <https://doi.org/10.1186/s40317-016-0109-4>, 2016.
- Palacios, D. M., Bailey, H., Becker, E. A., Bograd, S. J., DeAngelis, M. L., Forney, K. A., Hazen, E. L., Irvine, L. M., and
Mate, B. R.: Ecological correlates of blue whale movement behavior and its predictability in the California Current Ecosystem
615 during the summer-fall feeding season, *Mov Ecol*, 7, 26, <https://doi.org/10.1186/s40462-019-0164-6>, 2019.
- Parsons, T. T. and Strickland, J. D. H.: Discussion of spectrophotometric determination of marine-plant pigments, with revised
equations for ascertaining chlorophylls and carotenoids, *J Mar Res*, 21, 155–163, 1963.

- Paul, A. J., Coyle, K. O., and Ziemann, D. A.: Timing of spawning of *Thysanoessa raschii* (Euphausiacea) and occurrence of their feeding-stage larvae in an Alaskan Bay, *Journal of Crustacean Biology*, 10, 69–78, <https://doi.org/10.1163/193724090X00258>, 1990.
- 620
- Pearce, A., Hart, A., Murphy, D., and Rice, H.: Seasonal wind patterns around the Western Australian coastline and their application in fisheries analysis, Fisheries Research Report No. 266, last accessed November 1, 2024, https://www.fish.wa.gov.au/Documents/research_reports/fr266.pdf, 2015
- Plourde, S., Winkler, G., Joly, P., St-Pierre, J. F., and Starr, M.: Long-term seasonal and interannual variations of krill spawning in the lower St Lawrence estuary, Canada, 1979-2009, *J Plankton Res*, 33, 703–714, <https://doi.org/10.1093/plankt/fbq144>, 2011.
- 625
- Quartly, G. D., Aiken, J., Brewin, R. J. W., and Yool, A.: The link between surface and sub-surface chlorophyll-a in the centre of the Atlantic subtropical gyres: A comparison of observations and models, *Front Mar Sci*, 10, 1197753, <https://doi.org/10.3389/fmars.2023.1197753>, 2023
- 630
- Quetin, L. B. and Ross, R. M.: Environmental variability and its impact on the reproductive cycle of Antarctic krill, *Am Zool*, 41, 74–89, <https://doi.org/10.1093/icb/41.1.74>, 2001.
- R Core Team: R: A language and environment for statistical computing, last accessed September 19, 2023: <https://www.R-project.org/>, 2022.
- Rennie, S. J.: Oceanographic processes in the Perth Canyon and their impact on productivity, PhD, Curtin University of Technology, Perth, Western Australia, last accessed November 1, 2024: <https://espace.curtin.edu.au/handle/20.500.11937/1904>, 2005.
- 635
- Rennie, S. J., McCauley, R. D., and Pattiaratchi, C. B.: Thermal structure above the Perth Canyon reveals Leeuwin Current, undercurrent and weather influences and the potential for upwelling, *Mar Freshw Res*, 57, 849–861, <https://doi.org/10.1071/MF05247>, 2006.
- 640
- Rennie, S., Hanson, C. E., McCauley, R. D., Pattiaratchi, C., Burton, C., Bannister, J., Jenner, C., and Jenner, M. N.: Physical properties and processes in the Perth Canyon, Western Australia: Links to water column production and seasonal pygmy blue whale abundance, *Journal of Marine Systems*, 77, 21–44, <https://doi.org/10.1016/j.jmarsys.2008.11.008>, 2009a.
- Rennie, S. J., Pattiaratchi, C. B., and McCauley, R. D.: Numerical simulation of the circulation within the Perth Submarine Canyon, Western Australia, *Cont Shelf Res*, 29, 2020–2036, <https://doi.org/10.1016/j.csr.2009.04.010>, 2009b.
- 645
- Roesler, C. S. and Barnard, A. H.: Optical proxy for phytoplankton biomass in the absence of photophysiology: Rethinking the absorption line height, *Methods in Oceanography*, 7, 79–94, <https://doi.org/10.1016/j.mio.2013.12.003>, 2013.
- Roesler, C., Uitz, J., Claustre, H., Boss, E., Xing, X., Organelli, E., Briggs, N., Bricaud, A., Schmechtig, C., Poteau, A., D’Ortenzio, F., Ras, J., Drapeau, S., Haëntjens, N., and Barbieux, M.: Recommendations for obtaining unbiased chlorophyll estimates from *in situ* chlorophyll fluorometers: A global analysis of WET Labs ECO sensors, *Limnol Oceanogr Methods*, 650 15, 572–585, <https://doi.org/10.1002/lom3.10185>, 2017.

- van Ruth, P., Rodriguez, A. R., Davies, C., and Richardson, A. J.: Indicators of depth layers important to phytoplankton production, State and Trends of Australia's Ocean Report, <https://doi.org/10.26198/5e16a98549e7d>, 2020.
- Salgado Kent, C., Bouchet, P., Wellard, R., Parnum, I., Fouda, L., and Erbe, C.: Seasonal productivity drives aggregations of killer whales and other cetaceans over submarine canyons of the Bremer Sub-Basin, south-western Australia, *Aust Mammal*, 43, 168–178, <https://doi.org/10.1071/AM19058>, 2020.
- 655 Schmechtig, C., Claustre, H., Poteau, A., D'Ortenzio, F., Schallenberg, C., Trull, T. W., and Xing, X.: Biogeochemical-Argo quality control manual for chlorophyll-a concentration and chl-fluorescence, Version 3.0., <https://doi.org/10.13155/35385>, 2023.
- Schmidt, K., Atkinson, A., Venables, H. J., and Pond, D. W.: Early spawning of Antarctic krill in the Scotia Sea is fuelled by “superfluous” feeding on non-ice associated phytoplankton blooms, *Deep Sea Res 2 Top Stud Oceanogr*, 59–60, 159–172, <https://doi.org/10.1016/j.dsr2.2011.05.002>, 2012.
- 660 Scott, B. E., Sharples, J., Ross, O. N., Wang, J., Pierce, G. J., and Camphuysen, C. J.: Sub-surface hotspots in shallow seas: Fine-scale limited locations of top predator foraging habitat indicated by tidal mixing and sub-surface chlorophyll, *Mar Ecol Prog Ser*, 408, 207–226, <https://doi.org/10.3354/meps08552>, 2010.
- 665 Seegers, B. N., Stumpf, R. P., Schaeffer, B. A., Loftin, K. A., and Werdell, P. J.: Performance metrics for the assessment of satellite data products: An ocean color case study, *Opt Express*, 26, 7404, <https://doi.org/10.1364/OE.26.007404>, 2018.
- Smith, R. C.: Remote sensing and depth distribution of ocean chlorophyll, *Mar Ecol Prog Ser*, 5, 359–361, 1981.
- Speakman, C. N., Hoskins, A. J., Hindell, M. A., Costa, D. P., Hartog, J. R., Hobday, A. J., and Arnould, J. P. Y.: Environmental influences on foraging effort, success and efficiency in female Australian fur seals, *Sci Rep*, 10, 17710, <https://doi.org/10.1038/s41598-020-73579-y>, 2020.
- 670 Steele, J. H.: Environmental control of photosynthesis in the sea, *Limnol Oceanogr*, 7, 137–150, <https://doi.org/10.4319/lo.1962.7.2.0137>, 1962.
- Steele, J. H.: A study of production in the Gulf of Mexico, *J Mar Res*, 22, 211–222, 1964.
- Steinke, K. B., Bernard, K. S., Ross, R. M., and Quetin, L. B.: Environmental drivers of the physiological condition of mature female Antarctic krill during the spawning season: implications for krill recruitment, *Mar Ecol Prog Ser*, 669, 65–82, <https://doi.org/10.3354/meps13720>, 2021.
- Suryan, R. M., Santora, J. A., and Sydeman, W. J.: New approach for using remotely sensed chlorophyll *a* to identify seabird hotspots, *Mar Ecol Prog Ser*, 451, 213–225, <https://doi.org/10.3354/meps09597>, 2012.
- Sutton, A. L.: Krill in the Leeuwin Current system: Influence of oceanography and contribution to Indian Ocean zoogeography, PhD, Murdoch University, Perth, Western Australia, last accessed September 13, 2023: <https://researchportal.murdoch.edu.au/esploro/outputs/doctoral/Krill-in-the-Leeuwin-Current-system/991005544756707891>, 2015.
- 680 Sutton, A. L. and Beckley, L. E.: Influence of the Leeuwin Current on the epipelagic euphausiid assemblages of the south-east Indian Ocean, *Hydrobiologia*, 779, 193–207, <https://doi.org/10.1007/s10750-016-2814-7>, 2016.

- 685 The MathWorks Inc.: MATLAB version: 9.13.0 (R2022b), last accessed October 12, 2023:
https://www.mathworks.com/?s_tid=gn_logo, 2022.
- Thieurmel, B. and Elmarhraoui, A.: Suncalc: Compute sun position, sunlight phases, moon position, and lunar phase. R package version 0.5.1, last accessed September 19, 2023: <https://CRAN.R-project.org/package=suncalc>, 2022.
- Thompson, P. A., Pesant, S., and Waite, A. M.: Contrasting the vertical differences in the phytoplankton biology of a dipole
690 pair of eddies in the south-eastern Indian Ocean, *Deep Sea Res 2 Top Stud Oceanogr*, 54, 1003–1028,
<https://doi.org/10.1016/j.dsr2.2006.12.009>, 2007.
- Thompson, P. A., Bonham, P., Waite, A. M., Clementson, L. A., Cherukuru, N., Hassler, C., and Doblin, M. A.: Contrasting
oceanographic conditions and phytoplankton communities on the east and west coasts of Australia, *Deep Sea Res 2 Top Stud
Oceanogr*, 58, 645–663, <https://doi.org/10.1016/j.dsr2.2010.10.003>, 2011.
- 695 Thomson, P. G., Mantovanelli, A., Wright, S. W., and Pattiaratchi, C. B.: *In situ* comparisons of glider bio-optical
measurements to CTD water properties, in: *Australian Marine Sciences Conference: Estuaries to Oceans*, 306, 2015.
- Thums, M., Ferreira, L. C., Jenner C., Harris, D., Davenport, A., Andrews-Goff, V., Double, M., Möller, L., Attard, C. R. M.,
Bilgmann, K., Thomson, P. G., and McCauley, R.: Pygmy blue whale movement, distribution and important areas in the
Eastern Indian Ocean, *Global Ecol Conserv*, 35, e02054, <https://doi.org/10.1016/j.gecco.2022.e02054>, 2022.
- 700 Twomey, L. J., Waite, A. M., Pez, V., and Pattiaratchi, C. B.: Variability in nitrogen uptake and fixation in the oligotrophic
waters off the south west coast of Australia, *Deep Sea Res 2 Top Stud Oceanogr*, 54, 925–942,
<https://doi.org/10.1016/j.dsr2.2006.10.001>, 2007.
- Uitz, J., Claustre, H., Morel, A., and Hooker, S. B.: Vertical distribution of phytoplankton communities in open ocean: An
assessment based on surface chlorophyll, *J Geophys Res Oceans*, 111, C08005, <https://doi.org/10.1029/2005JC003207>, 2006.
- 705 Waite, A. M., Thompson, P. A., Feng, M., Beckley, L. E., Domingues, C. M., Gaughan, D., Hanson, C. E., Holl, C. M.,
Koslow, T., Meuleners, M., Montova J. P., Moore, T., Muhling, B. A., Paterson, H., Rennie, S., Strzelecki, J., and Twomey,
L.: The Leeuwin Current and its eddies: An introductory overview, *Deep-Sea Res Pt II*, 54, 789–796,
<https://doi.org/10.1016/j.dsr2.2006.12.008>
- Visser, F., Hartman, K. L., Pierce, G. J., Valavanis, V. D., and Huisman, J.: Timing of migratory baleen whales at the Azores
710 in relation to the North Atlantic spring bloom, *Mar Ecol Prog Ser*, 440, 267–279, <https://doi.org/10.3354/meps09349>, 2011.
- Weston, K., Fernand, L., Mills, D. K., Delahunty, R., and Brown, J.: Primary production in the deep chlorophyll maximum
of the central North Sea, *J Plankton Res*, 27, 909–922, <https://doi.org/10.1093/plankt/fbi064>, 2005.
- Whiteway, T.: Australian bathymetry and topography grid, June 2009. Scale 1:5000000,
<https://doi.org/10.4225/25/53D99B6581B9A>, 2009.
- 715 Woo, M. and Pattiaratchi, C.: Hydrography and water masses off the western Australian coast, *Deep-Sea Res Pt 1*, 55, 1090–
1104, <https://doi.org/10.1016/j.dsr.2008.05.005>, 2008
- Woo, L. M. and Gourcuff, C.: Delayed mode QA/QC best practice manual version 3.1, Integrated Marine Observing System
(IMOS), 1–60 pp., <https://doi.org/10.26198/5c997b5fdc9bd>, 2023.

- 720 Wu, J., Lee, Z., Xie, Y., Goes, J., Shang, S., Marra, J. F., Lin, G., Yang, L., and Huang, B.: Reconciling between optical and biological determinants of the euphotic zone depth, *J Geophys Res Oceans*, 126, e2020JC016874, <https://doi.org/10.1029/2020JC016874>, 2021.
- Yentsch, C. S. and Menzel, D. W.: A method for the determination of phytoplankton chlorophyll and phaeophytin by fluorescence, *Deep Sea Research and Oceanographic Abstracts*, 10, 221–231, [https://doi.org/10.1016/0011-7471\(63\)90358-9](https://doi.org/10.1016/0011-7471(63)90358-9), 1963.
- 725 Yoshida, T., Virtue, P., Kawaguchi, S., and Nichols, P. D.: Factors determining the hatching success of Antarctic krill *Euphausia superba* embryo: Lipid and fatty acid composition, *Mar Biol*, 158, 2313–2325, <https://doi.org/10.1007/s00227-011-1735-2>, 2011.